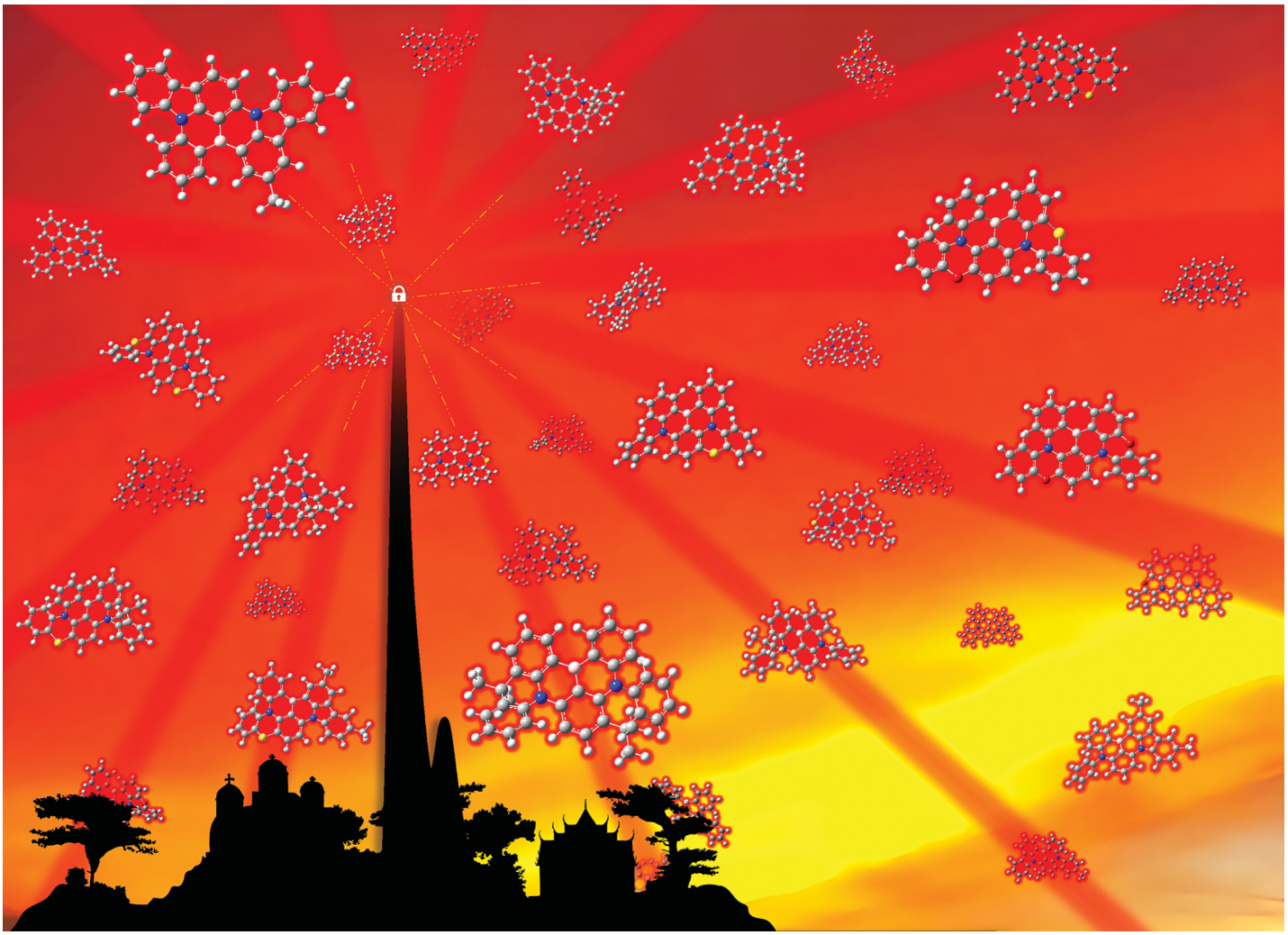

Showcasing research from the Group of Prof. Chuan-Kui Wang, Prof. Lili Lin, and Dr Zhongjie Wang, School of Physics and Electronics, Shandong Normal University, China

Multi-resonance thermally activated delayed fluorescence molecules with intramolecular-lock: theoretical design and performance prediction

Multi-resonance thermally activated delayed fluorescence (MR-TADF) molecules with narrow full width at half maximum (FWHM) have attracted much attention recently. In this work, 36 borane/amine (B/N) type MR-TADF molecules were theoretically designed by using intramolecular-lock strategy and systematically studied based on first-principles calculations. It is found that intramolecular-lock is an efficient strategy for the design of highly efficient MR-TADF emitters.

As featured in:

See Chuan-Kui Wang, Lili Lin, Zhongjie Wang *et al.*, *Phys. Chem. Chem. Phys.*, 2023, **25**, 24406.

ROYAL SOCIETY OF CHEMISTRY

rsc.li/pccp

Registered charity number: 207890

PCCP Owner Societies

PCCP

PAPER

View Article Online
View Journal | View Issue

Cite this: *Phys. Chem. Chem. Phys.*, 2023, **25**, 24406

Multi-resonance thermally activated delayed fluorescence molecules with intramolecular-lock: theoretical design and performance prediction†

Zhimin Wu, Qun Zhang, Xiaofei Wang, Kai Zhang, Xiaofang Li, Rui Li, Yuzhi Song, Jianzhong Fan, Chuan-Kui Wang,* Lili Lin* and Zhongjie Wang*

Received 17th May 2023,
Accepted 16th August 2023

DOI: 10.1039/d3cp02255b

rsc.li/pccp

Multi-resonance thermally activated delayed fluorescence (MR-TADF) molecules with narrow full width at half maximum (FWHM) have attracted much attention recently. In this work, 36 borane/amine (B/N) type MR-TADF molecules were theoretically designed by using an intramolecular-lock strategy and systematically studied based on first-principles calculations. It was found that intramolecular-lock at different positions and in different manners could induce different luminescent properties. The calculated oscillator strengths for PXZ-L_2 and PTZ-L_2 locking systems are weaker than that for 2DPABN (without intramolecular-lock), while the Cz-L_1 and TMCZ-L_1 locking could result in stronger oscillator strength. Though the calculated FWHM of all the systems with intramolecular-lock is higher than that of 2DPABN, the Cz, TMCz and DMAC locking at L_1 or L_2 would induce relatively small FWHM which is comparable to that of 2DPABN. Our calculation results indicate that intramolecular-lock could enhance the SOC values and decrease the energy gap between the first singlet excited state and the first triplet excited state, which is quite favorable to reverse intersystem crossing. The Cz, TMCz and DMAC locking systems could realize comparable and higher efficiency than 2DPABN, thus higher quantum efficiency could be obtained. Our calculation results indicate that the intramolecular-lock strategy is an effective method to realize the design of highly efficient MR-TADF emitters.

1. Introduction

Multi-resonance thermally activated delayed fluorescence (MR-TADF) materials have attracted much attention for application as light-emitting materials in organic light-emitting diodes (OLEDs).[1–6] Most traditional TADF molecules are composed of donors (D) and acceptors (A) with special hindrance, and a small energy gap (ΔE_{ST}) between the first singlet excited state (S_1) and the first triplet excited state (T_1) as well as efficient reverse intersystem crossing (RISC) can be realized.[7–12] However, D–A type TADF emitters suffer from significant structural relaxation in excited states and the large full width at half maximum (FWHM) of emission as well as a small radiative rate.[13] For this reason, the MR-TADF molecules which could realize spatial separation of the frontier molecular orbitals (FMOs) in fused planar boron–nitrogen (B–N) based polycyclic aromatic frameworks by the electron-deficient boron atom and the electron-rich nitrogen atom were first put forward by Hatakeyama *et al.*[14] This kind of design strategy enables the emitters to achieve both small ΔE_{ST} and suppressed structural relaxation in excited states, resulting in narrowband TADF emission and high photoluminescence quantum yields (PLQYs).[15–17] A series of high-performance MR-TADF molecules based on B–N polycyclic aromatic frameworks have been developed to prepare OLED materials, with extremely high color purity in the panchromatic tuning from blue to red[18–23] which was previously difficult to achieve for most traditional D–A type TADF molecules. So far, only two classes of molecules, borane/amine type (B/N) and amine/carbon type (N/C),[24–28] were found to have MR-TADF properties. More design strategies are needed to develop MR-TADF emitters. Recently, Wu and coworkers reported asymmetrical peripherally locking strategies on BN-based MR-TADF molecules, and obtained circularly polarized MR-TADF emitters with excellent luminescent properties.[18] The locking strategies have been successfully used in the D–A type TADF emitters to realize marked amplified spontaneous emission (ASE) by adjusting the torsion angles and restricting intramolecular relaxation.[29–31] However, the intramolecular-lock strategy applied to the MR-TADF emitters is quite limited. It is expected that the MR-TADF molecules with intramolecular-lock might present excellent luminescent properties.

Shandong Key Laboratory of Medical Physics and Image Processing & Shandong Provincial Engineering and Technical Center of Light Manipulations, School of Physics and Electronics, Shandong Normal University, Jinan 250358, China.
E-mail: ckwang@sdnu.edu.cn, linll@sdnu.edu.cn, wangzhongjie@sdnu.edu.cn

† Electronic supplementary information (ESI) available. See DOI: https://doi.org/10.1039/d3cp02255b

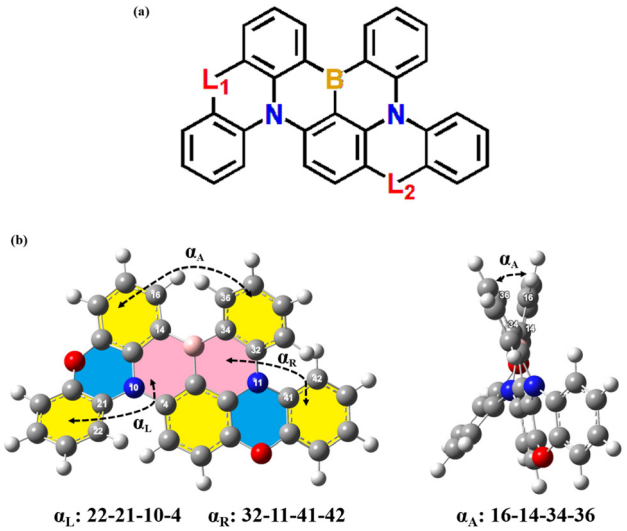

Fig. 1 Schematic diagram of the intramolecular-lock strategy for the studied molecules. (a) The schematic diagram of the dihedral angle (α_L), the dihedral angle (α_R), and the dihedral angle (α_A). (b).

In this work, 36 molecules were designed by using an intramolecular-lock strategy at different positions of the MR-TADF emitter 2-diphenylmethane-BN (2DPABN) with different positions or manners (as shown in Fig. 1(a) and 2). Based on our survey, five molecules including 10*H*-phenoxazine (PXZ), 10*H*-phenothiazine (PTZ), 9*H*-carbazole (Cz), 9,9-dimethyl-9,10-dihydroacridine (DMAC), and 1,3,6,8-tetramethyl-9*H*-carbazole (TMCz) locked at L_1 or (and) L_2 separately have been synthesized and studied as TADF emitters experimentally.[7,14,18,32–38] However, no theoretical study was performed on the intramolecular-lock strategy on the MR-TADF emitters. The relationship between geometric structures and photophysical properties of MR systems needs to be further explored. In this work, we would perform a systematic study on MR systems with different locking manners based on first-principles calculation and excited state decay rate analysis. The luminescent properties of 36 molecules are analyzed and potential MR-TADF emitters with high efficiency are predicted. This study would provide a reference for the design of MR-TADF molecules with highly efficient luminescent properties.

2. Theoretical methods and computational details

For all 36 molecules, S_1 and T_1 were optimized using the time-dependent density functional theory (TD-DFT) method. The optimization of the ground state (S_0) was performed with the density

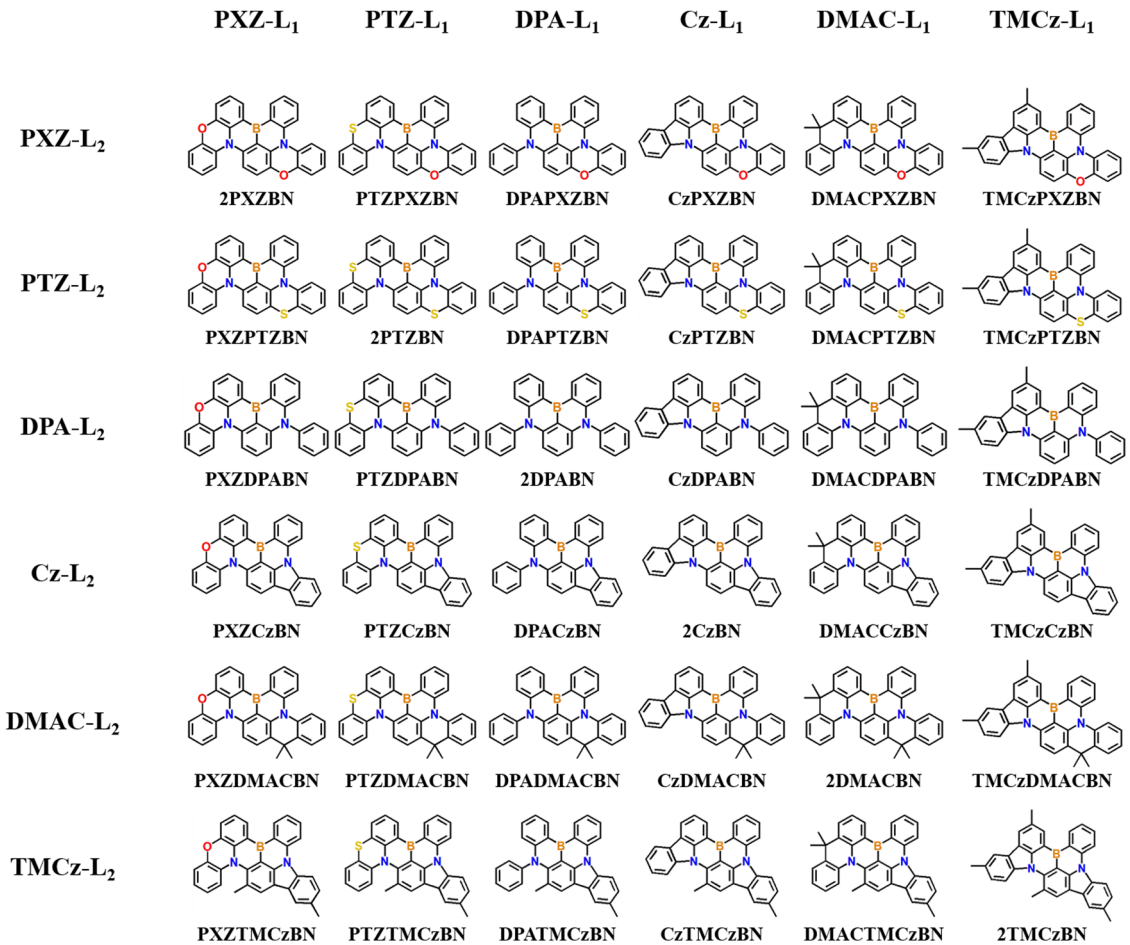

Fig. 2 Chemical structures of all studied molecules.

functional theory (DFT) method. The Hessian calculation was carried out to confirm that the local minimum of the potential energy is found for the three states. Six functionals (O3LYP, B3LYP, PBE0, PBE0-1/3, BMK and M062X) with different percentages of Hartree–Fock exchange (HF%) were tested. In Table 1, the absorption and emission wavelengths of eight molecules including 2PXZBN, 2DMACBN, 2DPABN, 2PTZBN, 2CzBN, 2TMCzBN, PTZDMACBN and DPACzBN were calculated. It is found that the results calculated with the O3LYP function showed better agreement with experimental values and were relatively more stable by comparing with the data calculated with other functionals. And more contrasting data are presented in Tables S1, S2 and Fig. S2 (ESI†). It should be noted that there are theoretical investigations showing that most common DFT functionals as well as the consideration of the Tamm–Dancoff approximation (TDA) consistently predict a much larger ΔE_{ST} owing to the absence of an explicit account of double (or higher order) excitations.[39,40] Our calculation based on O3LYP also shows a little larger value than experimental values, which is consistent with the results in ref. 39. However, we find that the tendency obtained from TD-DFT and spin-component scaling second-order approximate coupled-cluster (SCS-CC2) is similar as shown in Fig. S1 (ESI†) (data from in ref. 39). Considering the computational cost, we adopt O3LYP for further property prediction of MR-TADF emitters theoretically designed. In addition, the 6-31G(d) basis set which has been widely used in TADF emitters was adopted.[41–43] The polarizable continuum model (PCM) is used in our calculation to simulate the solvent environment, and all the calculations can be realized in the Gaussian 16 program.[44]

The variation of the geometric structure can be effectively determined by a geometric comparison between two states. The geometric difference between the two states is quantitatively shown in the root mean square displacement (RMSD) values, which can be displayed with Multiwfn.[45] The formula of RMSD is shown as:

$$\mathrm{RMSD} = \sqrt{\frac{1}{N}\sum_{i}^{n\mathrm{atom}}\left[\left(x_i - x_i'\right)^2 + \left(y_i - y_i'\right)^2 + \left(z_i - z_i'\right)^2\right]} \quad (1)$$

where i is the atomic ordinal number, x_i and x_i are the x coordinates of the ith atom, and y and z have the same meaning. The RMSD values of geometric structures of two states represent the change of the geometry in two states and reflect the degree of structural relaxation. If this value is large, the reorganization energy could be large and a fast nonradiative decay process may be resulted.

The radiative rate is calculated using the Einstein's spontaneous emission formula:

$$k_{\mathrm{r}} = \frac{f\Delta E_{\mathrm{fi}}{}^2}{1.499\ \mathrm{cm}^{-2}\ \mathrm{s}} \quad (2)$$

where f is the oscillator strength and ΔE_{fi} is the vertical emission energy between the initial state and the final state with the unit of wavenumbers (cm^{-1}).[46] Here the energy gap between S_1 and S_0 is used for fluorescence emission. It represents the decay rates of S_1 in the way of emission. Besides that, the S_1 state can also decay in the way of a nonradiative process which includes the internal conversion process and the intersystem crossing process to triplet states.

According to the Fermi's golden rule (FGR) and first-order perturbation theory, the nonradiative decay rate can be written as follows:

$$k_{\mathrm{nr}} = \frac{2\pi}{\hbar^2}\sum_{\mu,\nu} P_{\mathrm{i}\nu}\left|H_{\mathrm{f}\mu,\mathrm{i}\nu}\right|^2\delta\left(E_{\mathrm{i}\nu} - E_{\mathrm{f}\mu}\right) \quad (3)$$

where $P_{\mathrm{i}\nu}$ is the Boltzmann distribution function of the initial state. The letter i and f represent the initial and final electronic state, respectively. μ and ν are the label of vibrational states. $H_{\mathrm{f}\mu,\mathrm{i}\nu}$ is the interaction between two different Born–Oppenheimer states, and it contains two contributions as follows:

$$\hat{H}\Psi_{\mathrm{i}\nu} = \hat{H}^{\mathrm{BO}}\Phi_{\mathrm{i}}(r,Q)\Phi_{\nu}(Q) + \hat{H}^{\mathrm{SO}}\Phi_{\mathrm{i}}(r,Q)\Phi_{\nu}(Q) \quad (4)$$

Here $\hat{H}^{\mathrm{BO}}$ denotes the nonadiabatic coupling and $\hat{H}^{\mathrm{SO}}$ is the spin–orbit coupling. When the Fourier transform is applied for the delta function, the intersystem crossing rate constant between two electronic states with different spin multiplicity can be written as:

$$k_{\mathrm{ISC}} = \frac{1}{\hbar^2}\langle\Phi_{\mathrm{f}}|\hat{H}^{\mathrm{SO}}|\Phi_{\mathrm{i}}\rangle\int_{-\infty}^{\infty}\mathrm{d}t\left[\mathrm{e}^{i\omega_{\mathrm{if}}t}Z_i^{-1}\rho_{\mathrm{ISC}}(t,T)\right] \quad (5)$$

where Z_{i} is the partition function and $\rho_{\mathrm{ISC}}(t,T)$ is the thermal-vibration correlation function. The reverse intersystem crossing (RISC) rate can also be calculated using eqn (5). $\langle\Phi_{\mathrm{f}}|\hat{H}^{\mathrm{SO}}|\Phi_{\mathrm{i}}\rangle$ is the spin–orbit coupling (SOC) constant between two states with different spin multiplicity. SOC is a relativistic effect, which arises naturally in Dirac theory, a fully relativistic one-particle theory for spin 1/2 systems.[47] The SOC matrix elements between excited states can be evaluated as residues of quadratic response functions.[48,49] It can be calculated in the powerful molecular electronic structure program DALTON.[50,51] More details are added in the ESI† and we also refer to ref. 52. One should note that k_{IC} here means the internal conversion rate and k_{ISC} means the ISC rate. The molecular materials property prediction package (MOMAP) is used to calculate the ISC and RISC rates in toluene.[53–59] The detailed calculation information can be found in ref. 60.

3. Results and discussion

3.1 Geometric structures

The relative position between D and A has an important impact on the energy gap and excitation properties of TADF molecules. Here we adopt an intramolecular-lock strategy to lock the dihedral angles and form six different donors, thus the dihedral angles for the L_1-locking (α_L) and the L_2-locking (α_R) are shown in Fig. S3(a–f) (ESI†), and the angles (α_A) on triarylboron (TAB) of 36 molecules (optimized coordinates are listed in Table S3, ESI†) are also listed and illustrated in Fig. S3(g–i) and Table S4 (ESI†). The schematic diagram of α_L, α_R and α_A is shown in Fig. 1(b). It can be found that the value of α_L varies in the range of 11°–36° (except DPA-L_1 locking systems). α_R changes from 4° to 33° (except DPA-L_2 locking systems), and

Table 1 Emission wavelengths and absorption wavelengths were calculated using different functionals for the eight molecules in toluene. Experimental values are also listed (unit: nm)

		O3LYP	B3LYP	PBE0	PBE-1/3	BMK	M062X	Exp.
2PXZBN	Abs.	482	455	438	410	409	384	475[a]
	Emi.	532	498	478	445	441	412	504[a]
2DMACBN	Abs.	462	438	422	397	396	375	461[a]
	Emi.	504	473	454	425	421	396	485[a]
2DPABN	Abs.	421	402	389	368	368	352	437[b]
	Emi.	456	430	413	388	384	367	462[b]
2PTZBN	Abs.	480	451	434	406	402	379	471[a]
	Emi.	537	499	479	445	436	409	510[a]
2CzBN	Abs.	456	432	416	393	392	372	458[a]
	Emi.	482	453	435	408	406	385	477[a]
2TMCzBN	Abs.	468	443	427	403	402	381	491[a]
	Emi.	492	463	446	419	416	394	512[a]
PTZDMACBN	Abs.	471	444	427	401	398	376	467[c]
	Emi.	529	489	470	437	429	403	497[c]
DPACzBN	Abs.	442	420	406	383	382	365	450[a]
	Emi.	475	446	429	403	400	380	469[a]

[a] Measured in 1×10^{-5} M toluene solution at 300 K. [b] Measured in 2×10^{-5} M in CH_2Cl_2 at 300 K. [c] Measured in 1×10^{-5} M toluene solution at 298 K.

α_A is from 9° to 37° for all molecules in S_0, S_1 and T_1. It can also be seen that for DPA-L_1 and DPA-L_2 locking systems, the dihedral angles (α_L and α_R) are quite large. This indicates that the locking strategy can effectively confine the dihedral angles in the donor groups, while the angles in the acceptor have quite limited influence. Specifically, we find that the Cz- or TMCz- lock at both L_1 and L_2 would have a similar influence on α_A as DPA, while the PXZ-, PTZ- or DMAC- lock at L_1 and L_2 would induce higher α_A. This might be induced by the stronger structure modulation of TAB when a hexatomic ring is induced. Similar influence can be found for all three states. The angle difference would induce different planarity of donors and acceptors, which would also influence the charge transfer properties.

The root mean square displacement (RMSD) values are calculated to compare the difference between two states (S_0–S_1, S_0–T_1 or S_1–T_1) which can be shown in Fig. S4 (ESI†). and Fig. 3. It is found that the RMSD values between two excited states (S_1–T_1) are much smaller than the values involving the ground state and excited states (S_0–S_1 and S_0–T_1). It means that the geometric structures of two excited states are quite close to each other, which may also induce a small energy gap between them. From Fig. 3(a) and (b), we can find that the RMSD values for PXZ-L_2, PTZ-L_2 and DMAC-L_2 locking systems change only a little when the L_1-locking is different. It means that L_2-locking has more significant influence on the RMSD values. It can be found that PTZ-L_2 locking would induce relatively larger RMSD values, and the values in PXZ-L_2 and DMAC-L_2 locking systems are quite close to each other. The values for DPA-L_2, Cz-L_2 and TMCz-L_2 systems vary significantly, which means both L_1 and L_2 locking would have strong influence on the RMSD values. It can be found that the molecule 2CzBN with both Cz-L_1 and Cz-L_2 locking have the smallest RMSD values. The RMSD values could reflect the variation of the non-radiative rates to some extent.[61]

3.2 Photophysical properties

The calculated absorption and emission wavelengths of all 36 molecules are shown in Fig. 4. It is found that all the molecules with locked groups would have red-shift emission compared to the molecule without a locked group (2DPABN). The absorption wavelengths for the locked molecules are also larger than that for 2DPABN. In addition, both absorption and emission wavelengths for the molecules locked with PXZ and PTZ at L_2 are larger than those for molecules locked with DPA, Cz, DMAC and TMCz at L_2. The emission wavelength range of the molecules (locked by PXZ-L_2 and PTZ-L_2) is from 592 nm (DPAPXZBN) to 616 nm (PTAPXZBN). So, the MR-TADF molecules locked with PXZ or PTZ would induce more significant red-shift emission, and are potential TADF emitters with red emission. However, the molecules with DPA would have the smallest absorption and emission wavelengths. In addition, we find that the locking at the L_1 position has only a little influence on the absorption wavelength with the variation being smaller than 50 nm. For locking at L_2, the variation for all systems is close to 75 nm. It means that L_2 locking has more significant influence on the absorption wavelengths. Similar to the absorption wavelengths, L_2 locking has also more obvious influence on the emission wavelengths. The variation induced by L_2 locking is even larger than that in absorption wavelengths (close to 175 nm). It means that the locking strategy has more influence on S_1 than S_0.

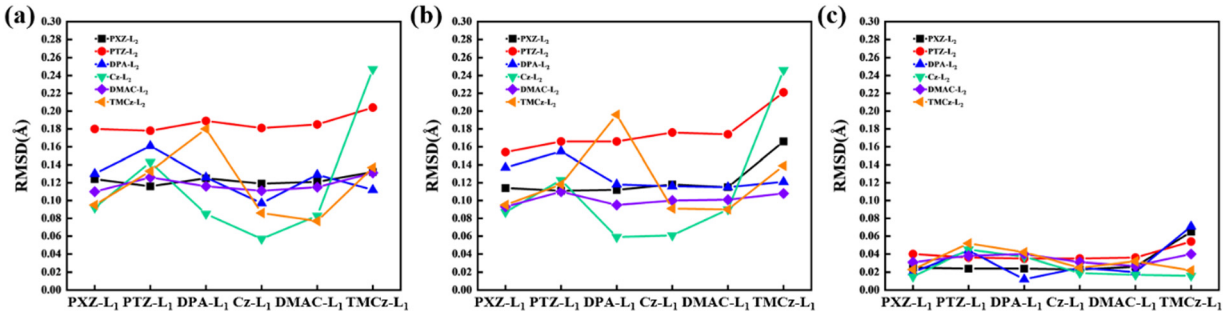

Fig. 3 Root mean square displacement (RMSD) for S_0–S_1 (a), S_0–T_1 (b) and S_1–T_1 (c) for all studied molecules by O3LYP/6-31G(d) in toluene.

The narrow full width at half maximum (FWHM) of emission is one important advantage for light-emitting materials in OLEDs. Here the FWHM is calculated as shown in Fig. 4(c) and Fig. S5 (ESI†). It is found that most of the molecules studied have a FWHM less than 80 nm, and the molecule 2DPABN without intramolecular lock can obtain the smallest FWHM value. It means that locking could induce larger FWHM. For PXZ-L_2 and PTZ-L_2 locked molecules, the FWHM values are relatively larger. It is concluded that the emission color would be less pure for the PXZ-L_2 or PTZ-L_2 locked molecules although they could realize redshift emission. This also reflects that it is also difficult to obtain emission with long wavelengths and narrow FWHM values using an intramolecular locking strategy. For Cz-L_2, TMCz-L_2 and DMAC-L_2 systems, the FWHM values are much smaller than the PTZ-L_2 and PXZ-L_2 locking systems. It can also be found that the PTZ-L_1 and PXZ-L_1 could also have a larger FWHM. It is concluded that Cz, TMCz and DMAC locking at L_1 or L_2 would induce relatively small FWHM. 2CzBN could have the smallest FWHM.

The energy gap between S_1 and T_1 (ΔE_{ST}) determines whether TADF can be realized by influencing the RISC process. The ΔE_{ST} values for 36 molecules are illustrated in Fig. 5(a) and Fig. S6 (ESI†). It is found that the energy gaps for all the systems are smaller than 0.4 eV. The values for PTZ-L_2 locking could strongly decrease the energy gap, followed by the PXZ-L_2 and DMAC-L_2 locking strategies. However, the PXZ-L_1 locked molecules are larger than other systems based on L1 locking. For L_1-locking, the Cz-L_1 locked systems have relatively smaller ΔE_{ST} than other systems. It is found that the molecule (CzPTZBN) with Cz-L_1 locking and PTZ-L_2 locking have the smallest energy gap. It is also found that most of the systems with intramolecular-locking have smaller energy gaps than 2DPABN. It means locking strategies are also a good strategy to obtain a smaller energy gap.

If both S_1 and T_1 are contributed mainly by the highest occupied molecular orbital (HOMO) and the lowest unoccupied molecular orbital (LUMO), the energy difference can be approximated as $\Delta E_{ST} = E(S_1) - E(T_1) = 2J(\phi, \phi^*)$. Here J is the exchange energy which can be expressed as $J(\phi, \phi^*) = \langle\phi(1)\phi^*(2)|e^2/r_{12}|\phi(2)\phi^*(1)\rangle$, where ϕ and ϕ^* are wavefunctions of transition orbitals. Here we can see that exchange energy and overlap are two factors that influence ΔE_{ST}. The electron distribution in the HOMO and LUMO that contributes to transition is shown in Fig. S7 (ESI†). It is found that there is no electron distribution on the N atom in the HOMO, while significant distribution is found in the LUMO. Short-range charge transfer can be observed in molecular orbitals. At the same time, the energy gap between the two orbitals (ΔE_{H-L}) is also listed in Table S5 (ESI†) and illustrated in Fig. S8 (ESI†), which shows a consistent rule with the absorption wavelengths. The transition properties of excited states can also be described with natural transition orbitals (NTOs) which are drawn in Fig. 6 and Fig. S9, Fig. S10 (ESI†) for S_1 and T_1. NTO is used to search for a compact orbital representation by multiple

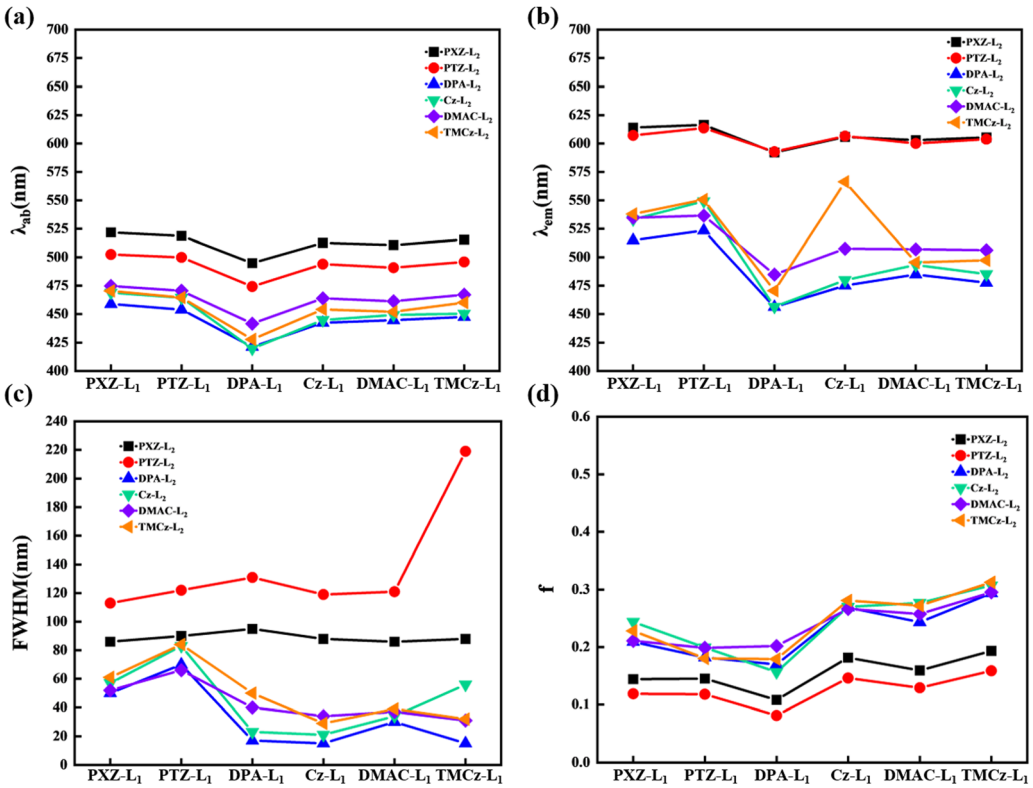

Fig. 4 Absorption wavelength (λ_{ab}) (a), emission wavelength (λ_{em}) (b), full width at half maximum (FWHM) of emission wavelength (c) and the oscillator strength (f) (d) for all studied molecules by O3LYP/6-31G(d) in toluene.

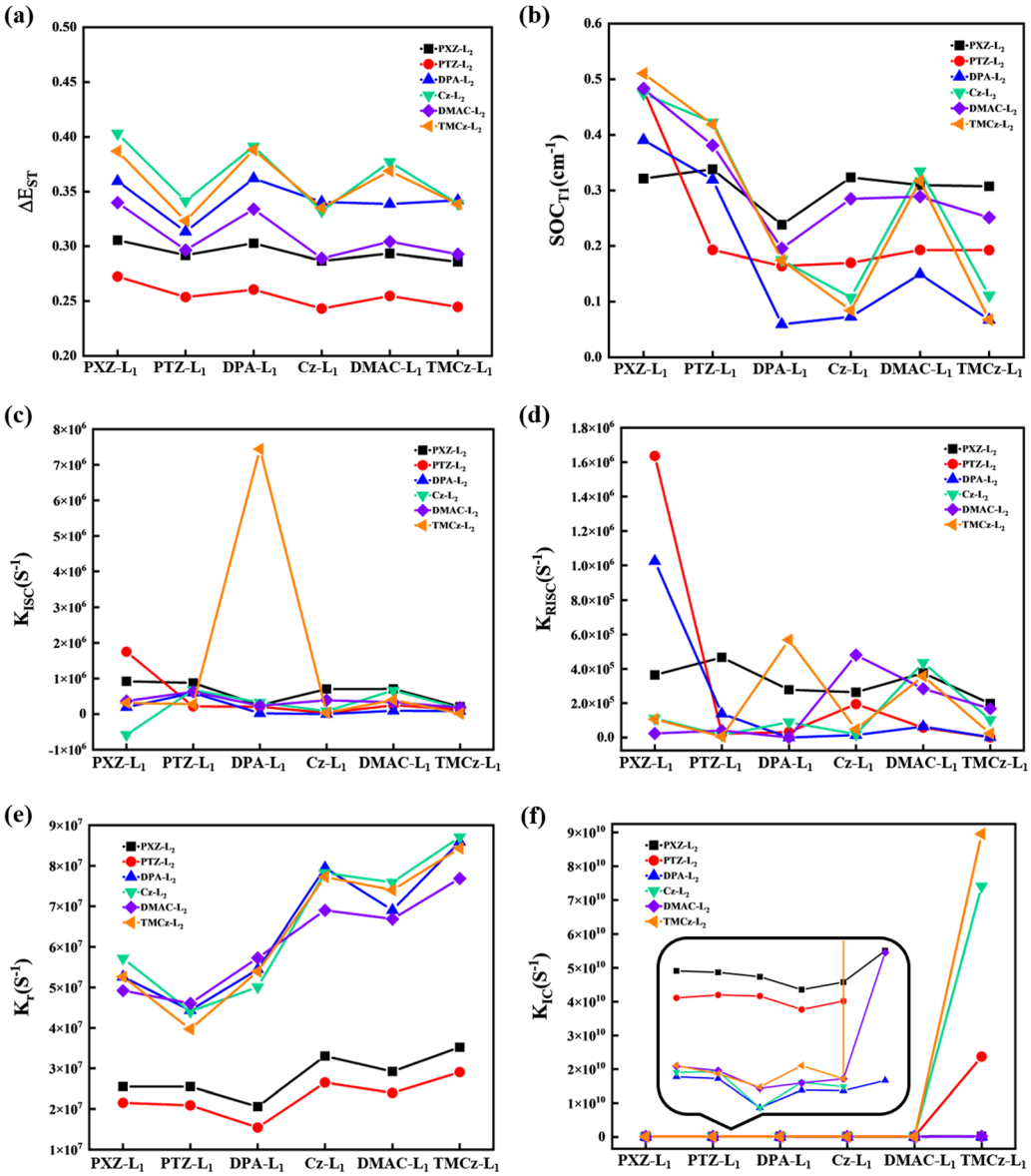

Fig. 5 Energy gap (ΔE_{ST}) (a), spin–orbit coupling (SOC) (b), intersystem crossing rates (k_{ISC}) (c) and reverse intersystem crossing rates (k_{RISC}) (d) between S_1 and T_1 for all studied molecules by O3LYP/6-31G(d) in toluene. The radiation rates (k_r) (e) and the internal conversion rates (k_{IC}) (f) between S_1 and S_0 for the studied twenty molecules by O3LYP/6-31G(d) in toluene.

orbital transition modes, when more than one pair of molecular orbits is involved in the transition. To quantitatively categorize the transition properties, the S_r index, which is the full space integral to the $S_r(r)$ functions, is defined as:

$$S_r \text{ index} = \int S_r(r)\mathrm{d}r \equiv \int \sqrt{\rho^{hole}(r)\rho^{ele}(r)}\mathrm{d}r \qquad (6)$$

Here ρ^{hole} is the hole density and ρ^{ele} is the electron density. We can define the transition properties of the excited state by analyzing the value S_r index which represents the particle-hole overlap. When the value is smaller than 40%, the overlap between electrons and holes is limited, which means significant charge transfer would occur in transition, and the state would be defined as a charge-transfer (CT) state. When the value is in the range 75–100%, a large orbital overlap can be observed and a large transition dipole moment would be obtained. This kind of state could be defined as a local-excited (LE) state. When the value is between 40% and 75%, a hybrid local-excited and charge transfer (HLCT) state is defined.[62–64] From NTOs, we can find that all MR-TADF molecules studied here have HLCT properties regardless of S_1 and T_1. The values are around 60% for both S_1 and T_1 in all the systems. From Fig. 6, we can see that Cz-L_2 and TMCz-L_2 locking would induce larger values, which means more localized excitation (LE) would occur during excitation. The PTZ-L_2 and PXZ-L_2 locking (with smaller values) would result in stronger charge transfer, while the Cz group plays a more significant role in inducing strong charge transfer for the L_1

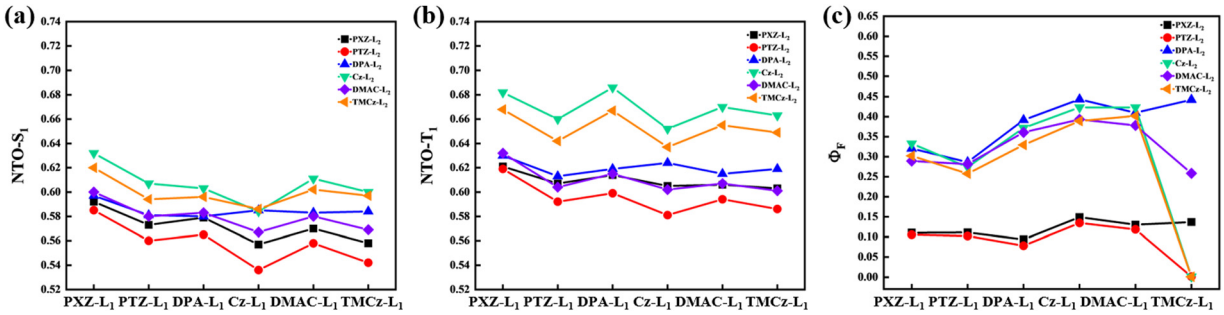

Fig. 6 Electron–hole overlap for S_1 (a) and T_1 (b) for all studied molecules by O3LYP/6-31G(d) in toluene. The fluorescence efficiency is illustrated in (c).

locking in both S_1 and T_1. In addition, the values for molecules in the T_1 state are all larger than those in S_1. The differences between Cz-L_2 or TMCz-L_2 systems and DPA-L_2 systems in T_1 are also large than that in S_1. The HLCT properties in all the MR systems would favor the generation of a small ΔE_{ST} and a large transition dipole moment, both of which are the most important requirements for TADF emitters. The oscillator strength (f) which has a close relationship with the transition dipole moment (TDM) is calculated and is shown in Fig. 4(d). It is found that the oscillator strengths for PTZ-L_2 and PXZ-L_2 locking systems are all smaller than other systems. This is consistent with the stronger CT properties in S_1 for PTZ-L_2 and PXZ-L_2 locking systems. For L_1 locking, the Cz-L_1 and TMCZ-L_1 would result in larger oscillator strength, which is good for luminescence.

3.3 Decay rates of excited states

In addition to ΔE_{ST}, the spin–orbit coupling (SOC) constant is another important parameter to characterize the process of up-conversion, and the values are shown in Fig. 5(b) and Table 2.[65,66] We can find that all the systems with intramolecular locking have larger SOC values than the molecule without locking (2DPZBN). The system with PXZ-L_1 locking has larger SOC values compared with other systems with L_1 locking, and systems with PXZ-L_2 locking also have relatively large SOC values. Consequently, the PXZ locking strategy is propitious to the ISC process for the MR-TADF molecules. In addition, we find that Cz-L_1 and TMCz-L_1 locking have weak enhancement on the SOC values than 2DPABN. The values of intersystem crossing rates (k_{ISC}) and reverse intersystem crossing rates (k_{RISC}) between S_1 and T_1 can directly characterize the ISC and RISC process between excited states, and the data for the 36 molecules are listed in Table 2 and Fig. 5(c) and (d). It is found that the systems with intramolecular-lock can obtain a larger k_{ISC} compared with 2DPABN except PXZCZBN. Similar results can be easily found in the RISC rate, which should have close relationship with the relatively smaller ΔE_{ST} in the systems with intramolecular-lock. In addition, we find that most RISC rates are comparable with the ISC rates with about one order of magnitude smaller except for 2DPABN, TMCzDPABN, DPADMACBN and PTZTMCzBN. This indicates that most molecules designed could realize up-conversion from T_1 to S_1, and are potential TADF emitters.

A high radiative rate (k_r) is one of the important conditions for efficient emission in TADF emitters. The calculated radiative rates for all the systems are listed in Table 2 and Fig. 5(e). It is found that TMCz-L_1 and Cz-L_1 locking systems can generally obtain large k_r values. while PXZ-L_2 and PTZ-L_2 locking systems would have smaller radiative rates which should be induced by the smaller overlap between holes and particles. The calculated radiative rates are about one or two orders of magnitude larger than the ISC rates, which satisfy the requirement for TADF. Another important factor to improve the fluorescence efficiency is a smaller internal conversion rate (k_{IC}). The calculated results are listed in Table 2 and Fig. 5(f). We can find that k_{IC} ($\sim 10^8$) is about an order of magnitude larger than k_r ($\sim 10^7$) for molecules studied in this work except for TMCzPTZBN, TMCzCzBN, and 2TMCzBN. The PTZ-L_2 and PXZ-L_2 locking systems have larger nonradiative rates than other systems (with values close to 2DPABN) except for TMCzBN, TMCzCzBN and TMCzPTZBN. This would directly influence fluorescence efficiency. The calculated fluorescence efficiency is shown in Fig. 6(c). It is found that the molecules with PTZ-L_2 and PXZ-L_2 locking have much smaller fluorescence efficiency than other intramolecular-lock systems (except for TMCzCzBN and 2TMCzBN). The fluorescence efficiency of Cz-L_2, TMCz-L_2 and DMAC-L_2 locking systems is close to that of 2DPABN. The calculated fluorescence efficiency of CzDPABN, 2CZBN, CzDMACBN, 2DMACBN and TMCZDPABN is larger than that of DPABN. This indicates that molecules with proper locking strategy could realize higher fluorescence efficiency. One could note that the calculated efficiency is smaller than the experimental values (close to 100% for some TADF emitters) due to the approximations used in theoretical calculation.

4. Conclusions

In summary, 36 MR molecules with intramolecular-lock are theoretically designed and studied. It is found that the locking position and locking manner have different influences on the luminescent properties. It is found that PXZ-, PTZ- or DMAC-locking at L_1 and L_2 would induce higher α_A due to the stronger structure modulation of TAB when a hexatomic ring is induced. Cz- or TMCz-locking at both L_1 and L_2 would have a similar influence on α_A to DPA. Both the calculated absorption and emission wavelengths are larger than those of 2DPABN with no intramolecular-lock. It means that intramolecular-lock could induce red-shift emission. However, the calculated FWHM of

Table 2 Spin–orbit coupling (SOC) between S_1 and T_1 calculated based on the geometry of T_1, the radiation rates (k_r) and internal conversion rates (k_{IC}) between S_1 and S_0 as well as the intersystem crossing rates (k_{ISC}), reverse intersystem crossing rates (k_{RISC}) between S_1 and T_1 and the values of fluorescence efficiency (Φ_F) for all studied molecules by O3LYP/6-31G(d) in toluene

	SOC_{T_1} (cm^{-1})	k_r (s^{-1})	k_{IC} (s^{-1})	k_{ISC} (s^{-1})	k_{RISC} (s^{-1})	Φ_{PF} (%)
2PXZBN	0.322	2.55×10^7	2.04×10^8	9.21×10^5	3.64×10^5	11.05
PTZPXZBN	0.338	2.55×10^7	2.03×10^8	8.75×10^5	4.66×10^5	11.12
DPAPXZBN	0.238	2.06×10^7	1.99×10^8	2.48×10^5	2.78×10^5	9.36
CzPXZBN	0.324	3.30×10^7	1.88×10^8	7.02×10^5	2.63×10^5	14.91
DMACPXZBN	0.310	2.92×10^7	1.94×10^8	7.08×10^5	3.76×10^5	13.03
TMCzPXZBN	0.307	3.52×10^7	2.22×10^8	2.06×10^5	1.98×10^5	13.69
PXZPTZBN	0.480	2.15×10^7	1.81×10^8	1.75×10^6	1.64×10^6	10.56
2PTZBN	0.193	2.09×10^7	1.83×10^8	2.13×10^5	2.10×10^4	10.24
DPAPTZBN	0.164	1.54×10^7	1.82×10^8	2.05×10^5	3.19×10^4	7.81
CzPTZBN	0.170	2.65×10^7	1.70×10^8	2.93×10^4	1.94×10^5	13.47
DMACPTZBN	0.193	2.40×10^7	1.78×10^8	2.49×10^5	5.71×10^4	11.86
TMCzPTZBN	0.192	2.91×10^7	2.37×10^{10}	1.29×10^5	9.44×10^2	0.12
PXZDPABN	0.391	5.26×10^7	1.11×10^8	1.91×10^5	1.02×10^6	32.03
PTZDPABN	0.319	4.43×10^7	1.10×10^8	5.95×10^5	1.38×10^5	28.64
2DPABN	0.059	5.44×10^7	8.46×10^7	2.15×10^4	1.20×10^2	39.16
CzDPABN	0.073	7.95×10^7	9.98×10^7	2.24×10^3	1.45×10^4	44.33
DMACDPABN	0.150	6.90×10^7	9.93×10^7	9.36×10^4	6.37×10^4	40.97
TMCzDPABN	0.068	8.59×10^7	1.08×10^8	8.13×10^4	2.04×10^3	44.23
PXZCzBN	0.474	5.72×10^7	1.15×10^8	-5.84×10^5	1.11×10^5	33.28
PTZCzBN	0.423	4.41×10^7	1.16×10^8	6.79×10^5	1.44×10^4	27.40
DPACzBN	0.175	5.01×10^7	8.43×10^7	3.26×10^5	8.95×10^4	37.17
2CzBN	0.108	7.82×10^7	1.07×10^8	8.07×10^4	1.92×10^4	42.31
DMACCzBN	0.335	7.59×10^7	1.03×10^8	6.63×10^5	4.36×10^5	42.32
TMCzCzBN	0.111	8.71×10^7	7.41×10^{10}	1.61×10^5	1.03×10^5	0.12
PXZDMACBN	0.483	4.92×10^7	1.21×10^8	3.69×10^5	2.30×10^4	28.91
PTZDMACBN	0.381	4.60×10^7	1.17×10^8	6.24×10^5	4.10×10^4	28.17
DPADMACBN	0.196	5.73×10^7	1.01×10^8	2.33×10^5	1.44×10^2	36.08
CzDMACBN	0.285	6.90×10^7	1.06×10^8	3.89×10^5	4.79×10^5	39.33
2DMACBN	0.289	6.68×10^7	1.10×10^8	3.31×10^5	2.84×10^5	37.81
TMCzDMACBN	0.251	7.68×10^7	2.20×10^8	1.84×10^5	1.67×10^5	25.84
PXZTMCzBN	0.510	5.26×10^7	1.21×10^8	3.14×10^5	1.07×10^5	30.21
PTZTMCzBN	0.419	3.97×10^7	1.14×10^8	2.77×10^5	5.45×10^3	25.77
DPATMCzBN	0.175	5.40×10^7	1.02×10^8	7.44×10^6	5.68×10^5	32.94
CzTMCzBN	0.084	7.72×10^7	1.21×10^8	3.50×10^4	4.75×10^4	38.92
DMACTMCzBN	0.317	7.40×10^7	1.10×10^8	3.97×10^5	3.57×10^5	40.19
2TMCzBN	0.068	8.43×10^7	8.96×10^{10}	1.49×10^4	2.33×10^4	0.09

the MR molecules with intramolecular-lock are a little larger than 2DPABN. But the Cz, TMCz and DMAC locking at L_1 or L_2 would induce relatively small FWHM which is comparable with that of 2DPABN. Our calculation results also indicate that intramolecular-lock could induce smaller energy gap and larger SOC values between S_1 and T_1, which is favorable for the generation of TADF. The calculated oscillator strength for PXZ-L_2 and PTZ-L_2 locking systems is weak than that for 2DPABN, while the Cz-L_1 and TMCZ-L_1 locking could result in stronger oscillator strength. The calculated radiative rates which have a close relationship with the oscillator strength show similar results. Based on the calculated fluorescence efficiency, we conclude that Cz, TMCz and DMAC locking systems could realize comparable and higher efficiency. All the calculated RISC rates are comparable to the ISC rates, which confirm the generation of TADF. In addition, we predict that a more efficient RISC process would be realized in systems with intramolecular-lock, thus higher quantum efficiency could be obtained for them. Our calculation results indicate that intramolecular-lock is a highly efficient strategy to enhance the fluorescence efficiency and quantum efficiency of MR-TADF molecules, which may favor the design of new type of MR-TADF molecules.

Conflicts of interest

There are no conflicts of interest to declare.

Acknowledgements

This work is supported by the National Natural Science Foundation of China (grant no. 11974216, 11874242, 21933002 and 11904210). The authors acknowledge the support from the Taishan Scholar Project of Shandong Province. We gratefully acknowledge HZWTECH for providing computation facilities.

References

1 A. Pershin1, D. Hall, V. Lemaur, J.-C. Sancho-Garcia, L. Muccioli, E. Zysman-Colman, D. Beljonne and Y. Olivier, Highly emissive excitons with reduced exchange energy in thermally activated delayed fluorescent molecules, *Nat. Commun.*, 2019, **597**, 1–5.

2 H. Uoyama, K. Goushi, K. Shizu, H. Nomura and C. Adachi, Highly efficient organic light-emitting diodes from delayed fluorescence, *Nature*, 2012, **492**, 234–238.

3 K. Goushi, K. Yoshida, K. Sato and C. Adachi, Organic light-emitting diodes employing efficient reverse intersystem

crossing for triplet-to-singlet state conversion, *Nat. Photonics*, 2012, **6**, 253–258.
4 Q. Zhang, B. Li, S. Huang, H. Nomura, H. Tanaka and C. Adachi, Efficient blue organic light-emitting diodes employing thermally activated delayed fluorescence, *Nat. Photonics*, 2014, **8**, 326–332.
5 H. Tanaka, K. Shizu, H. Nakanotani and C. Adachi, Dual intramolecular charge-transfer fluorescence derived from a phenothiazine-triphenyltriazine derivative, *J. Phys. Chem. C*, 2014, **118**, 15985–15994.
6 T. Hofbeck, U. Monkowius and H. Yersin, Highly efficient luminescence of Cu(I) compounds-TADF combined with short-lived phosphorescence, *J. Am. Chem. Soc.*, 2014, **137**, 399–404.
7 Y. T. Qiu, H. Xia, J. S. Miao, Z. Y. Huang, N. Q. Li, X. S. Cao, J. M. Han, C. J. Zhou, C. Zhong and C. L. Yang, Narrowing the electroluminescence spectra of multiresonance emitters for high-performance blue oleds by a peripheral decoration strategy, *ACS Appl. Mater. Interfaces*, 2021, **13**, 59035–59042.
8 L. L. Lin, L. Cai, J. Z. Fan and C. K. Wang, Electroluminescent mechanism of thermally activated delayed fluorescence emitters: conformational effect, *J. Phys. Chem. C*, 2018, **122**, 19953–19961.
9 W. Sun, S. Guo, C. Hu, J. Fan and X. Peng, Recent development of chemosensors based on cyanine platforms, *Chem. Rev.*, 2016, **116**, 7768–7817.
10 X. Xiong, F. Song, J. Wang, Y. Zhang, Y. Xue, L. Sun, J. Na, G. Pan, T. Lu and X. Peng, Thermally activated delayed fluorescence of fluorescein derivative for time-resolved and confocal fluorescence imaging, *J. Am. Chem. Soc.*, 2014, **136**, 9590–9597.
11 J. Lee, N. Aizawa, M. Numata, C. Adachi and T. Yasuda, Versatile molecular functionalization for inhibiting concentration quenching of thermally activated delayed fluorescence, *Adv. Mater.*, 2017, **29**, 1604856.
12 L. S. Cui, H. Nomura, Y. Geng, J. U. Kim and C. Adachi, Controlling singlet-triplet energy splitting for deep-blue thermally activated delayed fluorescence emitters, *Angew. Chem., Int. Ed.*, 2017, **56**, 1571–1575.
13 S. S. Kothavale and J. Y. Lee, Three- and Four-Coordinate, Boron-Based, Thermally activated delayed fluorescent emitters, *Adv. Opt. Mater.*, 2020, **8**, 2000922.
14 T. Hatakeyama, K. Shiren, K. Nakajima, S. Nomura, S. Nakatsuka, K. Kinoshita, J. P. Ni, Y. Ono and T. Ikuta, Ultrapure blue thermally activated delayed fluorescence molecules: efficient HOMO–LUMO separation by the multiple resonance effect, *Adv. Mater.*, 2016, **28**, 2777–2781.
15 S. Madayanad Suresh, D. Hall, D. Beljonne, Y. Olivier and E. Zysman-Colman, Multiresonant thermally activated delayed fluorescence emitters based on heteroatom-doped nanographenes: recent advances and prospects for organic light-emitting diodes, *Adv. Funct. Mater.*, 2020, **30**, 1908677.
16 Y. Kondo, K. Yoshiura, S. Kitera, H. Nishi, S. Oda, H. Gotoh, Y. Sasada, M. Yanai and T. Hatakeyama, Narrowband deep-blue organic light-emitting diode featuring an organoboron-based emitter, *Nat. Photonics*, 2019, **13**, 678–682.
17 X. Liang, Z. P. Yan, H. B. Han, Z. G. Wu, Y. X. Zheng, H. Meng, J. L. Zuo and W. Huang, Peripheral amplification of multi- resonance induced thermally activated delayed fluorescence for highly efficient OLEDs, *Angew. Chem., Int. Ed.*, 2018, **57**, 11316–11320.
18 X. G. Wu, J. W. Huang, B. K. Su, S. Wang, L. Yuan, W. Q. Zheng, H. Zhang, Y. X. Zheng, W. G. Zhu and P. T. Chou, Fabrication of circularly polarized MR-TADF emitters with asymmetrical peripheral-lock enhancing helical B/N-doped nanographenes, *Adv. Mater.*, 2022, **34**, 2105080.
19 J. A. Knöller, G. Y. Meng, X. Wang, D. Hall, A. Pershin, D. Beljonne, Y. Olivier, S. Laschat, E. Zysman-Colman and S. N. Wang, Intramolecular borylation via sequential b-mes bond cleavage for the divergent synthesis of B,N,B-doped Benzo[4]helicenes, *Angew. Chem., Int. Ed.*, 2020, **59**, 3156–3160.
20 S. M. Suresh, E. Duda, D. Hall, Z. Yao, S. Bagnich, A. M. Z. Slawin, H. Bässler, D. Beljonne, M. Buck, Y. Olivier, A. Köhler and E. Zysman-Colman, A deep blue B,N-doped heptacene emitter that shows both thermally activated delayed fluorescence and delayed fluorescence by triplet-triplet annihilation, *J. Am. Chem. Soc.*, 2020, **142**, 6588–6599.
21 F. Chen, L. Zhao, X. D. Wang, Q. Q. Yang, W. L. Li, H. K. Tian, S. Y. Shao, L. X. Wang, X. B. Jing and F. S. Wang, Novel boron- and sulfur-doped polycyclic aromatic hydrocarbon as multiple resonance emitter for ultrapure blue thermally activated delayed fluorescence polymers, *Sci. China: Chem.*, 2021, **64**, 547–551.
22 Y. W. Zhang, D. D. Zhang, J. B. Wei, Z. Y. Liu, Y. Lu and L. Duan, Multi-resonance induced thermally activated delayed fluorophores for narrowband green OLEDs, *Angew. Chem., Int. Ed.*, 2019, **58**, 16912–16917.
23 N. Ikeda, S. Oda, R. Matsumoto, M. Yoshioka, D. Fukushima, K. Yoshiura, N. Yasuda and T. Hatakeyama, Solution-processable pure green thermally activated delayed fluorescence emitter based on the multiple resonance effect, *Adv. Mater.*, 2020, **32**, 2004072.
24 X. Y. Cai, B. Gao, X. L. Li, Y. Cao and S. J. Su, Singlet-triplet splitting energy management via acceptor substitution: complanation molecular design for deep-blue thermally activated delayed fluorescence emitters and organic light-emitting diodes application, *Adv. Funct. Mater.*, 2016, **26**, 8042–8052.
25 J. M. Han, Y. Y. Chen, N. Q. Li, Z. Y. Huang and C. L. Yang, Versatile boron-based thermally activated delayed fluorescence materials for organic light-emitting diodes, *Aggregate*, 2022, **182**, 1–30.
26 H. J. Cheon, Y. S. Shin, N. H. Park, J. H. Lee and Y. H. Kim, Boron-based multi-resonance TADF emitter with suppressed intermolecular interaction and isomer formation for efficient pure blue OLEDs, *Small*, 2022, **18**, 2107574.
27 X. Li, Y. Z. Shi, K. Wang, M. Zhang, C. J. Zheng, D. M. Sun, G. L. Dai, X. C. Fan, D. Q. Wang, W. Liu, Y. Q. Li, J. Yu, X. M. Ou, C. Adachi and X. H. Zhang, Thermally activated delayed fluorescence carbonyl derivatives for organic light-emitting diodes with extremely narrow full width at

half-maximum, *ACS Appl. Mater. Interfaces*, 2019, **11**, 13472–13480.

28 J. M. Santos, D. Sun, J. M. Moreno-Naranjo, D. Hall, F. Zinna, S. T. J. Ryan, W. Shi, T. Matulaitis, D. B. Cordes, A. M. Z. Slawin, D. Beljonne, S. L. Warriner, Y. Olivier, M. J. Fuchter and E. Zysman-Colman, An S-shaped double helicene showing both multi-resonance thermally activated delayed fluorescence and circularly polarized luminescence, *J. Mater. Chem. C*, 2022, **10**, 4861–4870.

29 Y. Wada, H. Nakagawa, S. Matsumoto, Y. Wakisaka and H. Kaji, Organic light emitters exhibiting very fast reverse intersystem crossing, *Nat. Photonics*, 2020, **14**, 643–649.

30 C. Y. Chan, M. Tanaka, Y. T. Lee, Y. W. Wong, H. Nakanotani, T. Hatakeyama and C. Adachi, Stable pure-blue hyperfluorescence organic light-emitting diodes with high-efficiency and narrow emission, *Nat. Photonics*, 2021, **15**, 203–207.

31 J. M. Oh, C. C. Venters, C. Di, A. M. Pinto, L. L. Wan, I. Younis, Z. Q. Cai, C. Arai, B. R. So, J. Q. Duan and G. Dreyfuss, U1 snRNP regulates cancer cell migration and invasion in vitro, *Nat. Commun.*, 2020, **11**, 1–8.

32 M. L. Yang, S. Shikita, H. Min, I. S. Park, H. Shibata, N. Amanokura and T. Yasuda, Wide-range color tuning of narrowband emission in multi-resonance organoboron delayed fluorescence materials through rational imine/amine functionalization, *Angew. Chem., Int. Ed.*, 2021, **60**, 23142–23147.

33 P. C. Jiang, L. S. Zhan, X. S. Cao, X. L. Lv, S. L. Gong, Z. X. Chen, C. J. Zhou, Z. Y. Huang, F. Ni, Y. Zou and C. L. Yang, Simple acridan-based multi-resonance structures enable highly efficient narrowband green TADF electroluminescence, *Adv. Optical Mater.*, 2021, **9**, 1–7.

34 T. Hua, L. S. Zhan, N. Q. Li, Z. Y. Huang, X. S. Cao, Z. Q. Xiao, S. L. Gong, C. J. Zhou, C. Zhong and C. L. Yang, Heavy-atom effect promotes multi-resonance thermally activated delayed fluorescence, *Chem. Eng. J.*, 2021, **426**, 131169.

35 Z. M. Wu, Q. Zhang, X. F. Wang, K. Zhang, X. F. Li, Q. F. Mu, Y. Z. Song, J. Z. Fan, C. K. Wang and L. L. Lin, Theoretical study and molecular design of thermally activated delayed fluorescence molecules based on intramolecular-locked strategy, *J. Lumin.*, 2022, **251**, 119263.

36 Y. Kitamoto, T. Namikawa, T. Suzuki, Y. Miyata, H. Kita, T. Sato and S. Oi, Dimesitylarylborane-based luminescent emitters exhibiting highly-efficient thermally activated delayed fluorescence for organic light-emitting diodes, *Org. Electron.*, 2016, **34**, 216–225.

37 L. Ji, S. Griesbeck and T. B. Marder, Recent developments in and perspectives on three-coordinate boron materials: a bright future, *Chem. Sci.*, 2016, **8**, 846–863.

38 Z. M. Wu, F. Y. Li, Y. Zhou, J. Z. Fan and L. L. Lin, Structure-property relationship for triarylboron-based thermally activated delayed fluorescence molecules: A theoretical perspective, *Mater. Sci. Eng. B*, 2021, **270**, 115203.

39 D. Hall, J. C. Sancho-García, A. Pershin, G. Ricci, D. Beljonne, E. Zysman-Colman and Y. Olivier, Modeling of Multiresonant Thermally Activated Delayed Fluorescence Emitters—Properly Accounting for Electron Correlation Is Key!, *J. Chem. Theory Comput.*, 2022, **18**, 4903–4918.

40 M. Moral, L. Muccioli, W. J. Son, Y. Olivier and J. C. Sancho-García, Theoretical Rationalization of the Singlet−Triplet Gap in OLEDs Materials: Impact of Charge-Transfer Character, *J. Chem. Theory Comput.*, 2015, **11**, 168–177.

41 G. Y. Jiang, F. Y. Li, X. P. Kong, J. Z. Fan, Y. Z. Song, C. K. Wang and L. L. Lin, Suppression of aggregation caused quenching in U-shaped thermally activated delayed fluorescence molecules: *tert*-butyl effect, *J. Lumin.*, 2020, **219**, 116899.

42 Q. Peng and Z. G. Shuai, Molecular mechanism of aggregation-induced emission, *Aggregate*, 2021, **91**, 1–20.

43 Y. Im, M. Kim, Y. J. Cho, J. A. Seo, K. S. Yook and J. Y. Lee, Molecular design strategy of organic thermally activated delayed fluorescence emitters, *Chem. Mater.*, 2017, **29**, 1946–1963.

44 M. Frisch, G. Trucks, H. Schlegel, G. Scuseria, M. Robb, J. Cheeseman, G. Scalmani, V. Barone, G. Petersson and H. Nakatsuji, *Gaussian 16, Revision A.03*, Gaussian, Inc., Wallingford CT, 2016.

45 T. Lu and F. Chen, Multiwfn: a multifunctional wavefunction analyzer, *J. Comput. Chem.*, 2012, **33**, 580–592.

46 D. McCumber, Einstein relations connecting broadband emission and absorption spectra, *Phys. Rev.*, 1964, **136**, A954.

47 C. M. Marian, Spin-orbit coupling and intersystem crossing in molecules, *WIREs Comput. Mol. Sci.*, 2012, **2**, 187–203.

48 B. Minaev and H. Ågren, Theoretical DFT study of phosphorescence from porphyrins, *Chem. Phys.*, 2005, **315**, 215–239.

49 H. Ågren, O. Vahtras and B. Minaev, Response Theory and Calculations of Spin-Orbit Coupling Phenomena in Molecules, *Adv. Quantum Chem.*, 1996, **27**, 71–162.

50 K. Aidas, C. Angeli, K. L. Bak, V. Bakken, R. Bast, L. Boman, O. Christiansen, R. Cimiraglia, S. Coriani, P. Dahle, E. K. Dalskov, U. Ekström, T. Enevoldsen, J. J. Eriksen, P. Ettenhuber, B. Fernández, L. Ferrighi, H. Fliegl, L. Frediani, K. Hald, A. Halkier, C. Hättig, H. Heiberg, T. Helgaker, A. C. Hennum, H. Hettema, E. Hjertenæs, S. Høst, I.-M. Høyvik, M. F. Iozzi, B. Jansik, H. J. A. Jensen, D. Jonsson, P. Jørgensen, J. Kauczor, S. Kirpekar, T. Kjærgaard, W. Klopper, S. Knecht, R. Kobayashi, H. Koch, J. Kongsted, A. Krapp, K. Kristensen, A. Ligabue, O. B. Lutnæs, J. I. Melo, K. V. Mikkelsen, R. H. Myhre, C. Neiss, C. B. Nielsen, P. Norman, J. Olsen, J. M. H. Olsen, A. Osted, M. J. Packer, F. Pawlowski, T. B. Pedersen, P. F. Provasi, S. Reine, Z. Rinkevicius, T. A. Ruden, K. Ruud, V. Rybkin, P. Salek, C. C. M. Samson, A. Sánchez de Merás, T. Saue, S. P. A. Sauer, B. Schimmelpfennig, K. Sneskov, A. H. Steindal, K. O. Sylvester-Hvid, P. R. Taylor, A. M. Teale, E. I. Tellgren, D. P. Tew, A. J. Thorvaldsen, L. Thøgersen, O. Vahtras, M. A. Watson, D. J. D. Wilson, M. Ziolkowski and H. Ågren, The Dalton quantum chemistry program system, *WIREs Comput. Mol. Sci.*, 2014, **4**, 269–284.

51 Dalton, a molecular electronic structure program, **https://daltonprogram.org**.

52 L. H. Thomas B. A., I. The kinematics of an electron with an axis, *Phil. Mag.*, 1927, **3**, 1–22.

53 Z. G. Shuai, Thermal vibration correlation function formalism for molecular excited state decay rates, *Chin. J. Chem.*, 2020, **38**, 1223–1232.
54 Z. G. Shuai and Q. Peng, Excited states structure and processes: Understanding organic light-emitting diodes at the molecular level, *Phys. Rep.*, 2014, **537**, 123–156.
55 Q. Peng, Y. P. Yi, Z. G. Shuai and J. S. Shao, Excited state radiationless decay process with Duschinsky rotation effect: formalism and implementation, *J. Chem. Phys.*, 2007, **126**, 114302.
56 Y. Wang, Q. Peng, Q. Ou, S. Y. Lin and Z. G. Shuai, A novel molecular descriptor for highly efficient (ϕTADF > 90%) transition metal TADF Au(iii) complexes, *J. Mater. Chem. A*, 2020, **8**, 18721–18725.
57 K. Zhang, J. Z. Fan, C. K. Wang and L. L. Lin, Highly efficient T-shaped deep-red thermally activated delayed fluorescence emitters: substitution position effect, *Phys. Chem. Chem. Phys.*, 2021, **23**, 21883–21892.
58 J. Eng and T. J. Penfold, Understanding and designing thermally activated delayed fluorescence emitters: beyond the energy gap approximation, *Chem. Rec.*, 2020, **20**, 831–856.
59 F. M. Xie, J. X. Zhou, Y. Q. Li and J. X. Tang, Effects of the relative position and number of donors and acceptors on the properties of TADF materials, *J. Mater. Chem. C*, 2020, **8**, 9476–9494.
60 Y. L. Niu, W. Q. Li, Q. Peng, H. Geng, Y. P. Yi, L. J. Wang, G. J. Nan, D. Wang and Z. G. Shuai, MOlecular MAterials Property Prediction Package (MOMAP) 1.0: a software package for predicting the luminescent properties and mobility of organic functional materials, *Mol. Phys.*, 2018, **116**, 1078–1090.
61 F. Y. Li, G. Y. Jiang, M. Z. Li, J. Z. Fan, Y. Z. Song, C. K. Wang and L. L. Lin, Thermally activated delayed fluorescence emitters with dual conformations for white organic light-emitting diodes: mechanism and molecular design, *Phys. Chem. Chem. Phys.*, 2020, **22**, 1313–1323.
62 R. Chen, Y. Tang, Y. Wan, T. Chen, C. Zheng, Y. Qi, Y. Cheng and W. Huang, Promoting singlet/triplet exciton transformation in organic optoelectronic molecules: role of excited state transition configuration, *Sci. Rep.*, 2017, **7**, 6225.
63 A. D. Gorse and M. Pesquer, Intramolecular charge transfer excited state relaxation processes in para-substituted n,n-dimethylaniline: a theoretical study including solvent effects, *J. Phys. Chem.*, 1995, **99**, 4039–4049.
64 Y. Pan, W. Li, S. Zhang, L. Yao, C. Gu, H. Xu, B. Yang and Y. Ma, High yields of singlet excitons in organic electroluminescence through two paths of cold and hot excitons, *Adv. Opt. Mater.*, 2014, **2**, 510–515.
65 W. Li, D. Liu, F. Shen, D. Ma, Z. Wang, T. Feng, Y. Xu, B. Yang and Y. Ma, A twisting donor-acceptor molecule with an intercrossed excited state for highly efficient, deep-blue electroluminescence, *Adv. Funct. Mater.*, 2012, **22**, 2797–2803.
66 S. Ji, J. Ge, D. Escudero, Z. Wang, J. Zhao and D. Jacquemin, Molecular structure-intersystem crossing relationship of heavy-atom-free BODIPY triplet photosensitizers, *J. Org. Chem.*, 2015, **80**, 5958–5963.

